PURPOSE-LED PUBLISHING™

LETTER • OPEN ACCESS

Changes and drivers of vegetation productivity in China's drylands under climate change

View the article online for updates and enhancements.

You may also like

ENVIRONMENTAL RESEARCH
LETTERS

LETTER

Changes and drivers of vegetation productivity in China's drylands under climate change

Wenxin Zhou[1,2] , Changjia Li[1,2,*] , Bojie Fu[1,2], Shuai Wang[1,2], Zhuobing Ren[1,2] and Lindsay C Stringer[3,4]

[1] State Key Laboratory of Earth Surface Processes and Resource Ecology, Faculty of Geographical Science, Beijing Normal University, Beijing, People's Republic of China
[2] Institute of Land Surface System and Sustainable Development, Faculty of Geographical Science, Beijing Normal University, Beijing, People's Republic of China
[3] Department of Environment and Geography, University of York, York, United Kingdom
[4] York Environmental Sustainability Institute, University of York, York, United Kingdom
[*] Author to whom any correspondence should be addressed.

E-mail: changjia.li@bnu.edu.cn

Abstract

Increasing aridity can sharply reduce vegetation productivity in drylands, but elevated CO_2 and warming can enhance vegetation growth. However, the extent to which these positive effects counteract the negative effects of heightened aridity on vegetation productivity remains uncertain. Here, we used space-for-time substitution to assess the responses of 15 ecosystem variables to aridity in China's drylands and predicted vegetation productivity under future aridity, temperature, precipitation, nitrogen deposition, and CO_2. The results showed that vegetation productivity decreased abruptly as aridity (1-precipitation/potential evapotranspiration) increased to the threshold of 0.7, which corresponds to the vegetation decline stage in the dryland ecosystem's response to increasing aridity. Future projections suggest that 12.8% of China's drylands will cross aridity thresholds (0.7, 0.8, and 0.95) by 2100, in which vegetation productivity will significantly increase by 40.0%. Elevated CO_2 will stimulate vegetation growth, but continuously rising temperature and CO_2 by 2100 will have adverse effects, particularly in regions with limited nitrogen and water. This study suggests that effective adaptation and mitigation actions should be developed for regions crossing aridity thresholds, to ensure that drylands maintain the capacity to provide essential ecosystem services required to support the increasing population.

1. Introduction

Drylands, defined as regions with an aridity index (AI) below 0.65, represent areas where the mean annual precipitation is outweighed by the mean annual potential evapotranspiration (Mirzabaev *et al* 2019). In China, drylands cover a vast area of approximately 657.5×10^4 km², comprising approximately 66% of the country's land area (Li *et al* 2021), home to 580 million people (7% of the global population) (van der Esch 2017). These areas provide essential ecosystem services such as water and food, soil nutrients, and biodiversity conservation, but are highly vulnerable (Huang *et al* 2018) to desertification triggered by climate change and human activities (D'Odorico *et al* 2013, Huang *et al* 2017, Li *et al*

2023). Desertification poses significant challenges to water resources, food security, and carbon sequestration in China's drylands (Wang *et al* 2008), and nearly one-third of global dryland expansion is attributed to the expansion of Chinese drylands (Prăvălie *et al* 2019). Monitoring ecosystem indicators, such as vegetation productivity and soil nutrient levels, plays a crucial role in detecting land degradation and combating desertification onset in these regions (Berdugo *et al* 2017).

Field-based studies in China's drylands have identified abrupt, non-linear changes in ecosystem attributes in response to aridification (Wang *et al* 2014, Luo *et al* 2016, Hu *et al* 2021) For example, Wang *et al* (2014) observed a hump-shaped correlation between soil N isotopic values and aridity, with a peak

occurring at an aridity level of 0.68. Similarly, Hu *et al* (2021) found a shift in the dominant role of plant species diversity in soil microbial diversity and soil multifunctionality at an aridity level of 0.8. These findings underscore the strong correlation between key ecosystem variables and aridity but also reveal challenges in detecting thresholds across extensive gradients due to the limitations of field sampling, such as practical constraints, limited data collection, and lack of temporal coverage. (Maestre *et al* 2012, Berdugo *et al* 2022b). To overcome these limitations, the integration of data from remote sensing and published studies offer a practical solution for constructing large-scale datasets and proxies for ecosystem structure and function (Abel *et al* 2019, Smith *et al* 2019, Hillebrand *et al* 2020, Berdugo *et al* 2022a).

Given the significant role of drylands in global carbon cycles and their susceptibility to climate change (Yao *et al* 2020), understanding the dynamics of vegetation productivity is crucial. While previous studies using satellite remote sensing have identified notable greening trends in the northern drylands of China (Fu *et al* 2024), browning trends have been observed in the drylands of the southwestern United States and Australia (Wang *et al* 2022). Human land-use practices, such as afforestation, contribute to greening trends, whereas natural factors, including climate change, CO_2 fertilization, and nitrogen deposition, also play a role in vegetation productivity changes (Piao *et al* 2020, Wang *et al* 2022). For instance, trends and fluctuations in precipitation and temperature influence variations in plant water availability (Higgins *et al* 2023). Nitrogen availability is crucial for plant growth, with insufficient nitrogen utilization impeding growth and excess nitrogen-enhancing growth in nitrogen-limited systems (Greaver *et al* 2016). The rapid increase in potential evapotranspiration due to global warming exceeds that of precipitation, leading to atmospheric aridity (Jianping Huang *et al* 2016). Concurrently, a substantial escalation in atmospheric CO_2 levels has been found to alleviate the negative effects of aridification caused by global warming on vegetation growth (Zhang *et al* 2020). Elevated CO_2 levels result in CO_2 fertilization, enhancing photosynthesis by increasing substrate concentration and decreasing competition with O_2 at Rubisco reaction sites (Sellers *et al* 1996, O'Ishi *et al* 2009, Donohue *et al* 2013). Particularly in regions with limited water availability, an increase in CO_2 concentration triggers the partial closure of stomata in plants, maintaining the leaf-internal to ambient CO_2 concentration ratio, thereby enhancing water use efficiency (Sellers *et al* 1996, Lian *et al* 2021). Consequently, plant growth may still be promoted even under arid atmospheric conditions. Nonetheless, the positive effects of heightened CO_2 levels on plant growth are moderated by other environmental factors, such as constraints imposed

by soil water availability and essential nutrients such as nitrogen and phosphorus (Reich *et al* 2014, Wang *et al* 2020). The influence of environmental factors on vegetation is intricate, and its response to climate change remains debatable. Especially, as ecosystems transition across aridity thresholds, indicating vulnerability to sudden shifts in ecosystem structure and function, the degree to which increased CO_2 can counteract the adverse effects of aridification on vegetation remains uncertain.

Predicting vegetation dynamics and their primary driving forces in hotspot regions crossing aridity thresholds due to climate change will enhance our understanding of climate-vegetation interactions and carbon cycles, facilitating policymakers and land managers to adapt their management approaches to mitigate dryland degradation. Earth system models (ESMs) are essential tools for this task, as they integrate interactions between the atmosphere, biosphere, and human activities to project how aridity and vegetation productivity will change under various climate scenarios (Flato 2011, Bonan and Doney 2018). The Shared Socioeconomic Pathways (SSPs) framework within ESMs outlines potential future scenarios based on different levels of greenhouse gas emissions and socio-economic development (Rohat *et al* 2018). Research using ESMs indicates that high-emission scenarios may lead to significant declines in vegetation productivity in arid regions due to increased aridity (Lian *et al* 2021). However, some models suggest that elevated CO_2 could partially mitigate these losses, especially in lower-emission scenarios (Piao *et al* 2020). However, the extent of this mitigation remains uncertain, particularly due to potential limitations imposed by nutrient availability and other environmental factors.

In this study, we evaluated how 15 indicators from remote sensing datasets and meta-analysis datasets change along a wide aridity gradient in China's drylands. We integrated predictions from Coupled Model Intercomparison Project Phase 6 (CMIP6) models on future climate and vegetation dynamics to identify regions where future aridity will cross critical thresholds, analyze the trends in future vegetation productivity, and evaluate the key environmental factors driving vegetation changes. The objectives were to: (1) identify thresholds of key ecosystem attributes in response to increasing aridity, (2) identify spatial hotspots where critical aridity thresholds will be crossed by 2100, and (3) predict the trend of multi-year average summer gross primary productivity (GPP) changes and determine the dominant driving factors influencing changes in GPP in threshold-crossing regions through CMIP6 models. Identifying abrupt changes in the correlation between aridity and ecosystem indicators exposes significant vulnerabilities of dryland ecosystems to global climate change. Understanding vegetation dynamics

and their drivers is fundamental for enhancing and informing dryland management under the increasing pressures of climate change.

2. Materials and methods

2.1. Data collection
We selected variables that were important for determining key ecosystem attributes and processes, including nutrient cycling, plant productivity, biotic interactions, biodiversity, climatic patterns, soil health, and land degradation (Berdugo *et al* 2020, Wu *et al* 2020). Generally, these variables characterize three primary ecosystem components and processes: soils, plants, and plant–soil interactions (table 1). These variables were instrumental in assessing the response of ecosystem structure and function to increasing aridity and in identifying aridity thresholds. The variables were mainly sourced from interpolated data, remote sensing data, and information extracted from the published literature. To ensure temporal consistency when calculating aridity thresholds, we predominantly opted for time series datasets covering the period 1980–2015 for averaging. In cases where such time series were unavailable, we selected the closest available time series. For single-period data, such as the contents of soil organic carbon and soil nitrogen, as well as soil texture, which exhibits minimal short-term variability, the absence of drastic changes within the short term justified their use even without a complete time series spanning 1980–2015. Interpolated and remote sensing data were acquired by sampling points at 12 arc-minute intervals from freely accessible global maps. We specifically focused on sample points within China's drylands (AI < 0.65), discarding those classified as urban, cultivated land, or water bodies by the FAO. This process resulted in 12 450 remaining points for the analysis (figure S1). The variables extracted at each point and the data retrieved from published literature are described in table 1.

To assess vegetation dynamics and their driving factors in drylands under future climate change, we derived simulated precipitation, potential evapotranspiration, GPP, surface air temperature, surface-atmosphere CO_2, and nitrogen deposition simulation datasets from monthly mean products from 3 CMIP6 models with 16 variants (table S1), which are the only collections available. Nitrogen deposition includes the dry and wet deposition of NH_3, NH_4, and NO_y (total reactive nitrogen) (Matson *et al* 2002). These simulations include SSPs covering SSP1-2.6 (strong climate change mitigation), SSP2-4.5 (moderate mitigation), SSP3-7.0 (no mitigation baseline), and SSP5-8.5 (no mitigation, worst case) scenarios, respectively. The simulated data cover the period from 1980 to 2100, with a spatial resolution of 250 km, which is the highest resolution available that includes the required variables. Variables were bilinearly interpolated to 10 km subsets and aggregated to a yearly timescale. GPP, precipitation, temperature, CO_2, and nitrogen deposition data were extracted from the monthly data for summer, defined as June–August (Zhang *et al* 2022b).

2.2. Methods
The value obtained by subtracting the AI from 1 was used to represent aridity in this study. Therefore, the representation of aridity in drylands spans from 0.35 to 1, with elevated aridity values denoting heightened aridity levels. Assessing responses to aridity involved fitting relationships between all scrutinized ecosystem variables and aridity (table 1) using both linear and non-linear methods, such as general additive models (GAM) (Manzoni *et al* 2008). We treated the linear model as a null model, assuming a gradual response of a given ecosystem attribute as aridity increases. GAM model reveals a nonlinear but continuous pattern across the aridity gradient. The optimal fit for each scenario was determined using the Akaike information criterion (AIC). AIC acts as a benchmark for evaluating the complexity of statistical models and gauging their adequacy of fit of statistical models (Cavanaugh and Neath 2019). The model with the lowest AIC value, signifying the best fit, was capable of explaining the data most effectively while employing the fewest free parameters.

We investigated the presence of thresholds by examining non-linear regressions that provided a better fit to the data. Thresholds can be of two types: continuous or discontinuous, denoting a gradual or abrupt change in a variable with environmental pressure, respectively. We applied threshold models such as segmented, step, and stegmented (supporting information), to identify these thresholds, using AIC criteria to determine the best model and its corresponding threshold. The R packages *chngpt* and *gam* were used to apply segmented/step/stegmented and GAM regressions, respectively. However, these regressions do not necessarily indicate critical shifts, for which time-series analysis is required. To determine the optimal number of homogeneous threshold groups, we employed the cluster analysis by Elbow method, which use an analysis of the within-cluster sum of squares for various cluster numbers (Team RDC 2008). These thresholds were then organized into phases. We utilized aridity maps derived from CMIP6 climate models to identify regions likely to surpass the primary aridity thresholds identified because of the escalating aridity driven by climate change.

Partial correlation analysis was used to evaluate the partial correlation between GPP and one of the environmental factors (precipitation, temperature, CO_2, and nitrogen deposition) after controlling for other factors (Jiao *et al* 2021, Zhang *et al* 2022b). Cross convergent mapping (Sugihara *et al* 2012) is

Table 1. Description and origin of the map variables used in this study.

Variable typology	Variables taken	Description	References	Spatial resolution	Temporal resolution
Climate	Aridity index	The ratio of annual precipitation to annual potential evapotranspiration. Data is derived from the global aridity index (Global-Aridity) and global potential evapo-transpiration (Global-PET) geospatial database.	(Trabucco and Zomer 2018)	30 arc-secs	1970–2000, yearly
Climate	Inter-annual precipitation variability	Coefficient of variation of interannual precipitation. Data is derived from the TerraClimate 1980–2015 datasets.	(Abatzoglou *et al* 2018)	4 km	1980–2015, yearly
Soil	Soil organic carbon	Soil organic carbon content interpolated from ISRIC-WISE soil property databases.	(Batjes 2016)	30 arc-secs	1988–2015
Soil	Soil nitrogen content	Soil nitrogen content interpolated from ISRIC-WISE soil property databases.	(Batjes 2016)	30 arc-secs	1988–2015
Soil	Silt + Clay content	Silt + Clay content interpolated from ISRIC-WISE soil property databases.	(Batjes 2016)	30 arc-secs	1988–2015
Vegetation	Normalized difference vegetation index (NDVI)	NDVI quantifies vegetation by measuring the difference between near-infrared (which vegetation strongly reflects) and red light (which vegetation absorbs). Data is derived from MODIS (MOD13Q1 product) between January 2000 and December 2015	(Tucker and Sellers 1986)	250 m	2000–2015, monthly
Vegetation	Gross primary productivity (GPP)	Gross primary productivity is the rate at which solar energy is captured in sugar molecules during photosynthesis. Data is derived from MODIS (MOD17A2 product) between January 2000 and December 2015	(Running *et al* 2015)	500 m	2000–2015, monthly
Vegetation	Vegetation fraction cover	Fractional cover of trees and non-trees vegetation cover as interpolated from MODIS products. Data is derived from MODIS (MOD44B product).	(Justice *et al* 2002)	250 m	2000–2015, monthly
Vegetation	Root-shoot ratio	Data derived from a global database involving 3051 root-shoot ratio measurements, covering 1879 forest, 998 grassland, and 174 shrubland sites in China's drylands.	(Ma *et al* 2021)	30 arc-secs	1960–2020
Vegetation	Biocrust cover	Global distribution of biocrusts obtained by application of environmental niche modeling based on field observations described in more than 500 publications and identification of 18 independent environmental parameters controlling the suitability of the land surface for the growth of biocrust.	(Rodriguez-Caballero *et al* 2018)	1 km	1976–2015
Vegetation	Plant species richness	Plant species richness is calculated by [Native species richness—anthropogenic species Loss + Anthropogenic species increase (Species Invasions + Crop Species + Ornamental Species)].	(Ellis *et al* 2012)	0.05 °	Anthropocene

(Continued.)

Table 1. (Continued.)

Vegetation	Vegetation sensitivity index	Vegetation sensitivity to climate fluctuations. Data derived from the vegetation sensitivity index is the relative variance of vegetation productivity (enhanced vegetation index, EVI) with that of three ecologically important MODIS-derived climate variables (air temperature, water availability, and cloud cover) between 2000 and 2013 (database at LEFT project: www.left.ox.ac.uk/).	(Seddon *et al* 2016)	5 km	2000–2013, yearly
Vegetation	Sensitivity of vegetation to precipitation	Sensitivity of vegetation to precipitation is the slope of the regression between NDVI and precipitation. The index could reflect changes in the structural and functional ecosystem state that lead to environmental deterioration.	(Li *et al* 2021)	1 km	1982–2015, monthly
Vegetation	Aboveground carbon density and belowground carbon density	Data is derived from the dataset that covers the main dryland ecosystems including forests, grasslands, farmland, and shrublands.	(Xu *et al* 2020b)	Interpolated to 10 km	2010s
Ecosystem	Water yield, habitat quality, soil conservation, and carbon sequestration	Key ecosystem functions that drylands provided	(Xu *et al* 2020a)	1 km	2010, 2020

implemented to identify if the environmental factors are causing changes in vegetation productivity (supporting information, figures S16–S19). The largest absolute value of the partial correlation coefficient reflects the dominant driver affecting GPP variation.
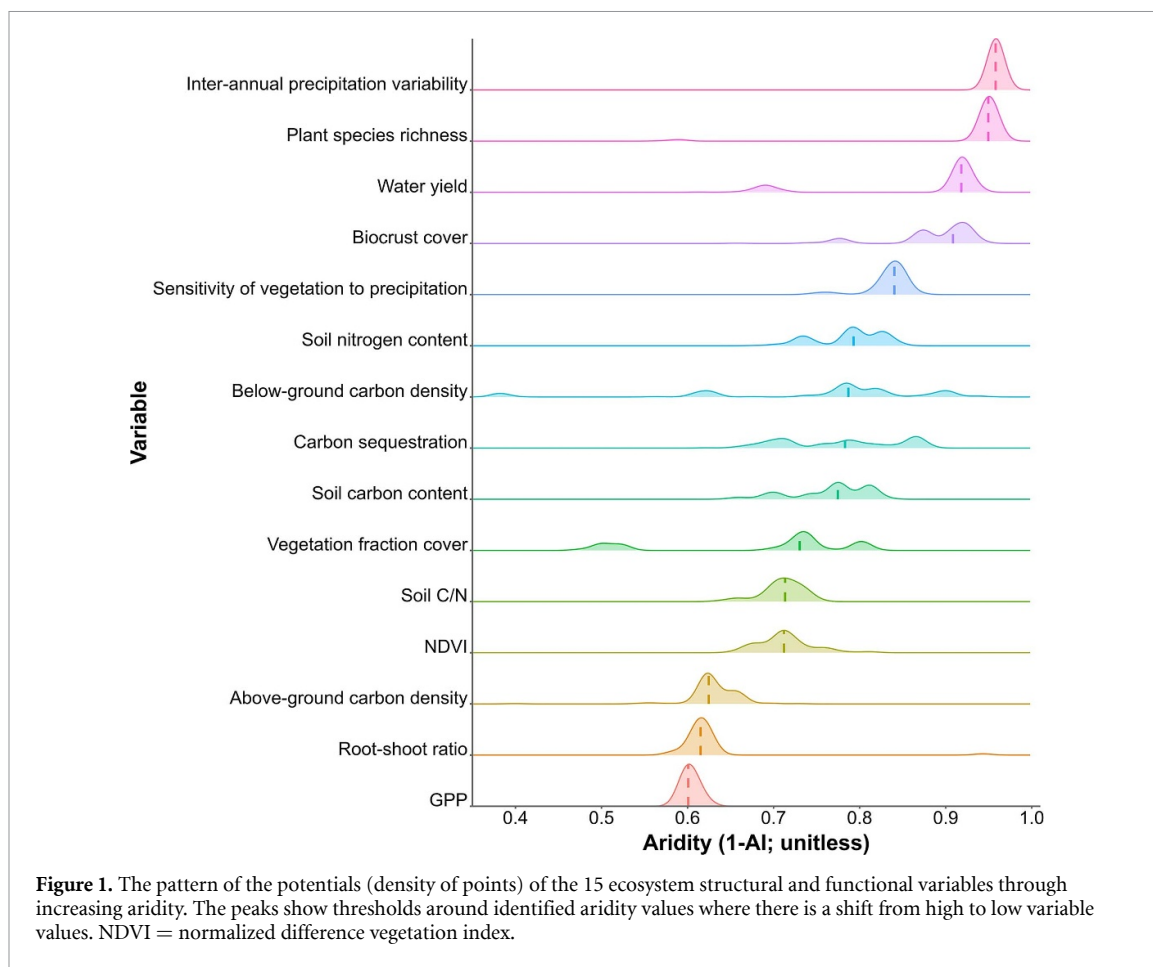
3. Results

3.1. Aridity thresholds for multiple ecosystem attributes

The majority of functional and structural ecosystem attributes exhibited a non-linear response to changes in aridity (figure 1). This implies that incremental increases in aridity levels can trigger substantial alterations in ecosystem variables once a critical aridity threshold is surpassed. Three distinct clusters were identified based on their most frequent cluster assignment, with centroids occurring at aridity values of 0.70, 0.80, and 0.95. These findings suggest that abrupt shifts in ecosystem dynamics in response to aridity can be categorized into three phases, each associated with a specific aridity threshold. The first group (*Phase 1*) was marked by a sharp decline in GPP, normalized difference vegetation index (NDVI), vegetation cover, and aboveground carbon density. The second group (*Phase 2*) exhibited an abrupt reduction in soil organic carbon, soil nitrogen content, belowground carbon density, and carbon sequestration. The third group (*Phase 3*)

was characterized by an abrupt increase in biocrust cover, inter-annual precipitation variability, and an abrupt decline in plant species richness and vegetation sensitivity index.

3.2. Hotspots for crossing critical aridity thresholds

For future projections, the mean aridity will increase to values of 0.72–0.74 in 2100, under the four SSPs (figure S5(A)). Compared to the historical period (1980–2014), drylands in China will expand by 18 721 km² and 47 567 km² during 2020–2060 and 2061–2100, respectively (figure S5(B)). According to the simulations, expansion will mainly occur in the northeastern regions, whereas shrinkage will occur mainly in the southwestern Qinghai–Tibet Plateau areas (figure S6). Among the four dryland subtypes, dry sub-humid, and arid drylands are expected to show the largest increase, accounting for 89% of the total dryland expansion (figures S7 and S8). According to the average of CMIP6 SSP1-2.6, 2–4.5, 3–7.0, and 5–8.5 scenarios, 12.8% of the current dryland area (0.8 million km²) will cross the three aridity thresholds identified by 2100 (figure 2). In areas forecasted to surpass the 0.8 aridity threshold, the anticipated impacts will be notably severe, covering the greatest area (0.6 million km²; 8.8% of drylands) and are mainly distributed in China's northeastern drylands.

Figure 1. The pattern of the potentials (density of points) of the 15 ecosystem structural and functional variables through increasing aridity. The peaks show thresholds around identified aridity values where there is a shift from high to low variable values. NDVI = normalized difference vegetation index.

### 3.3. GPP variation and the dominant driving factors

Compared with the historical period (1980–2014), 58.1% of the threshold-crossing region (238 301 km^2, with a 19.6% significant increase area, $p < 0.05$) will experience an increase in GPP for the timespan 2020–2060 under the SSP2-4.5 scenario (figure S10(A)). Considering the 2061–2100 period, the percentage of area with GPP increases will reduce to 31.7% (a significant increase area of 5.3%) (figure S10(B)). Under the SSP5-8.5 scenario, from 2020 to 2060, the area with GPP increases will be 149 393 km^2 larger compared to the SSP2-4.5 scenario. 80.1% of the area will exhibit a GPP increase, and 34.7% of the area will experience a significant GPP increase ($p < 0.05$) (figure S10(C)). 40 years later, the proportion of threshold-crossing regions with GPP increases will decrease to 65.4% (a significant increase area of 40.0%) (figure S10(D)).

In the SSP2-4.5 scenario, between 2020 and 2060, CO_2 and precipitation will predominantly drive GPP changes, accounting for 26.4% and 27.8%, respectively (figure 3(A)). However, between 2061 and 2100, the declining GPP trend is primarily driven by nitrogen deposition (20.1%) and precipitation (18.6%) (figure 3(B)). Under the SSP5-8.5 scenario, from 2020 to 2060, temperature (25.2%), CO_2 (14.4%), nitrogen deposition (19.1%), and precipitation (21.5%) will

drive the increase in GPP (figure 3(C)). 40 years later, CO_2 and nitrogen deposition will be the dominant drivers of GPP increases, with proportions of 20.2% and 19.5%, respectively (figure 3(D)).

4. Discussion

We found that gradual changes in aridification would lead ecosystem attributes to shift abruptly when the aridity value crosses critical thresholds (figure 1). Similar to prior empirical and quantitative analyzes of global dryland ecosystem thresholds driven by aridity, the response of China's drylands to increasing aridity exhibits three distinct phases (Phase 1–3) with abrupt shifts in various ecosystem structural and functional variables. These phases are delineated by abrupt declines in productivity, soil fertility, and plant richness at aridity values of 0.7, 0.8, and 0.95, respectively. *Phase 1* primarily involves vegetation decline, as plants typically reduce leaf area to cope with dry conditions (Berdugo *et al* 2022b). Vapour pressure deficit increases prompts plants to close stomata and modify leaf growth (e.g. increase specific leaf area), thereby weakening photosynthesis (Mansfield and Freer-Smith 1984). Other changes observed beyond the 0.7 aridity threshold include an increase in the root-shoot ratio (figure 1), likely associated with vegetation shifts from grasslands and
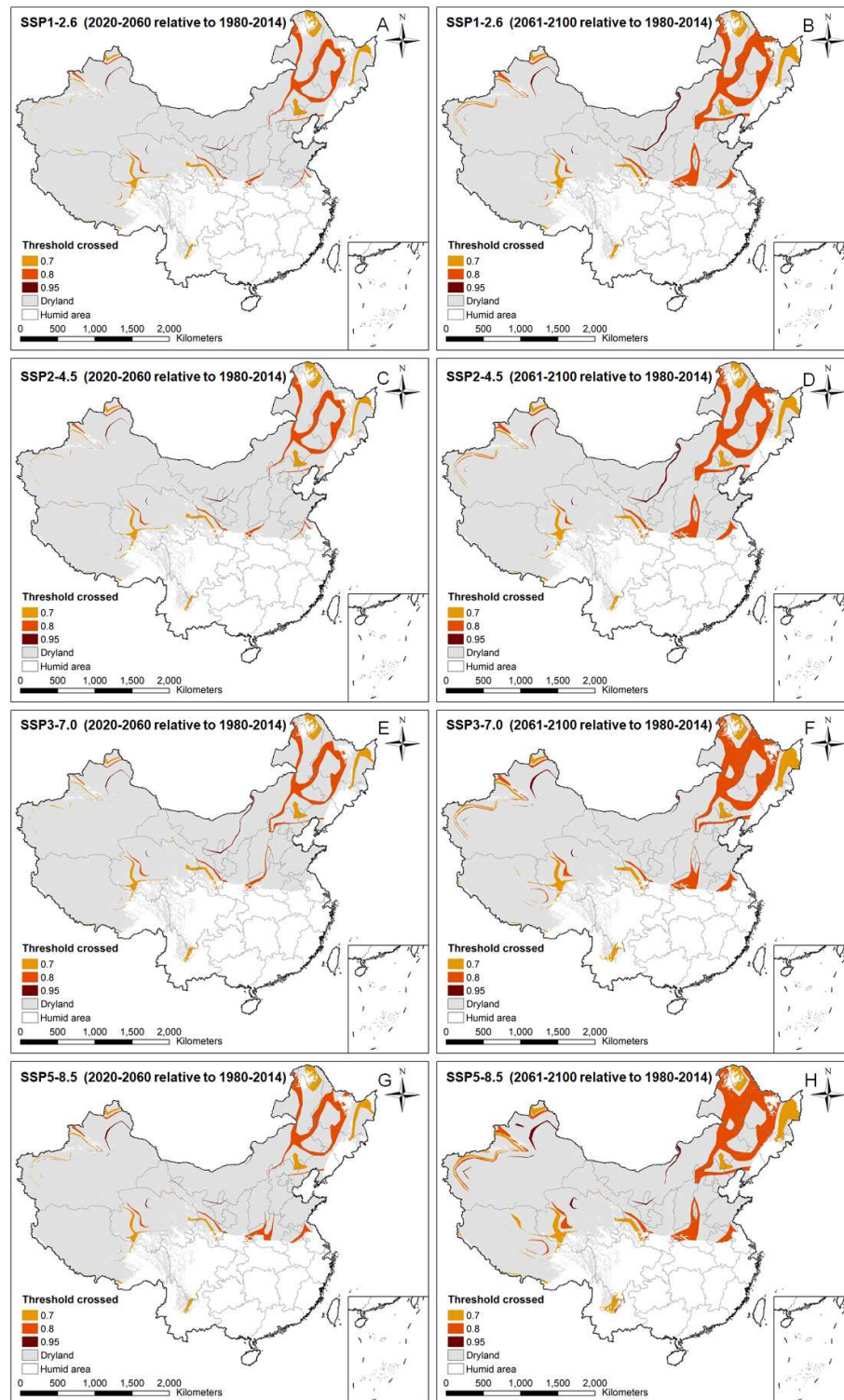
Figure 2. Predicted areas that will cross one or several of the aridity thresholds by the CMIP6 climate scenarios relative to the baseline period of 1980–2014 in China's drylands: SSP1-2.6 (strong climate change mitigation) for (A) 2020–2060 and (B): 2061–2100, SSP2-4.5 (moderate mitigation) for (C) 2020–2060 and (D) 2061–2100, SSP3-7.0 (no mitigation baseline) for (E) 2020–2060 and (F) 2061–2100, and SSP5-8.5 (no mitigation, worst case) for (G) 2020–2060 and (H) 2061–2100. The grey shading denotes the baseline drylands in 1950–2000, derived from the global aridity index database (Trabucco and Zomer 2018). Unshaded areas are not drylands today and therefore are outside of the range.

savannahs to deep-rooted species such as shrubs, better adapted to water-limited and nutrient-poor soils. *Phase 2* is likely to result from soil disruption, as reductions in vegetation cover and aboveground plant biomass during *Phase 1* diminish plant-derived organic inputs into the soil and related soil carbon and nitrogen contents. *Phase 3* is marked by an exponential rise in inter-annual variation in precipitation and biocrust cover compared to vascular plant cover. Rainfall is extremely variable in drylands, and
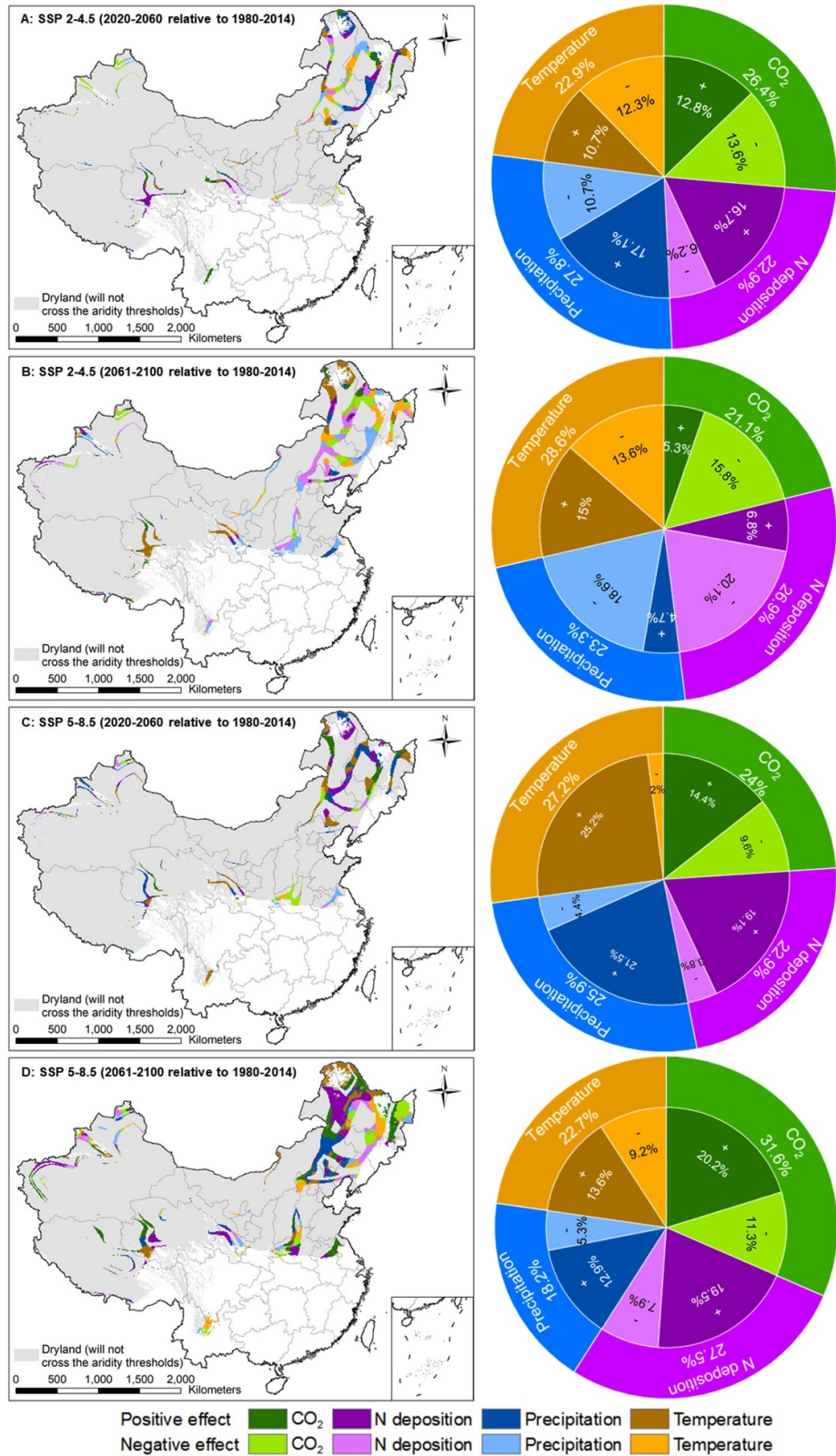
Figure 3. Spatial distribution and proportional distribution of dominance areas of the dominant driver of summer mean gross primary productivity (GPP) trend, by the CMIP6 climate scenarios relative to the baseline period of 1980–2014 in predicted areas that will cross one or several of the aridity thresholds: SSP2-4.5 (moderate mitigation) for (A) 2020–2060 and (B) 2061–2100, SSP5-8.5 (no mitigation, worst case) for (C) 2020–2060 and (D) 2061–2100. The dominant driver is defined as the driver that contributes the most to the increase (positive effect) or decrease (negative effect) in GPP in each grid cell. Grey shading denotes the baseline drylands in 1950–2000, derived from the global aridity index database (Trabucco and Zomer 2018). Unshaded areas are not drylands today and therefore are outside of the range.

it is expected to become even more variable as aridity increases (Berdugo *et al* 2020). Rapid increases in biocrust cover could mitigate the negative effects of reduced plant cover and biomass (Maestre *et al* 2016, Rodriguez-Caballero *et al* 2018). Most plant species struggle to survive water and nutrient shortages beyond an aridity level of 0.95, which is manifested by significant decreases in plant species richness and vegetation sensitivity.

However, we found different aridity thresholds for the three phases compared with previous assumptions, which posited aridity values of 0.54, 0.7, and 0.8, respectively (Berdugo *et al* 2020). Our findings revealed that the aridity thresholds for soil disruption (*Phase 2*) and systematic breakdown (*Phase 3*) phases are 0.8 and 0.95, respectively, which correspond to the transition between semi-arid and arid areas (AI or 1–aridity as 0.20), and the transition between arid and hyper-arid areas (AI or 1–aridity as 0.05), respectively. This study is in agreement with that reported by Hu *et al* (2021), who observed a shift in the relationship between plant or microbial diversity and soil multifunctionality at the semiarid-arid and arid climate boundary (around an aridity level of ~0.8), which is attributed to the significant influence of soil moisture on the surface climate conditions (Huang *et al* 2017). These results underscore the heightened sensitivity and vulnerability of transitional climate regions to climate change.

Climate projections indicate an increased risk of aridification in China's drylands under different climate scenarios based on SSPs in CMIP6 (figures S4–S7), which is consistent with the prediction of Jianping Huang *et al* (2016) based on CMIP5 simulations. Yao *et al* (2020) indicated that the expansion of drylands usually occurs on the boundary of drylands (aridity = 0.35) by transforming humid areas into dry sub-humid areas. However, we found that the shift from semi-arid to arid regions, specifically the crossing of the aridity threshold of 0.8, is also noteworthy (figures S4–S7). The regions projected to surpass the aridity thresholds of 0.8 and 0.95 (figure 2) are particularly sensitive, potentially experiencing significant soil disruption and loss of plant species. (Berdugo *et al* 2020). We found dryland expansion in northeast China will accelerate, which requires urgent and comprehensive measures to mitigate the potential impacts of aridification on ecosystems, socioeconomic aspects, and people's livelihoods.

The projected results regarding future changes in GPP suggest that in regions crossing the critical aridity thresholds (i.e. 0.7, 0.8, and 0.95), the proportion of areas exhibiting an increasing trend in GPP will be greater under the SSP5-8.5 scenario than under the SSP2-4.5 scenario. However, comparing the periods 2060–2100 and 2020–2060 under both scenarios, the proportion of area showing an increasing trend in GPP will decrease (figure S9). This implies that global

warming and elevated CO_2 concentrations may have a stimulating effect on vegetation growth, including enhanced metabolism (Braswell *et al* 1997), a CO_2 fertilization effect (Sellers *et al* 1996), and improved water-use efficiency due to elevated CO_2 concentrations (Lian *et al* 2021). However, as temperatures continue to rise and CO_2 concentrations continue to increase, this could have adverse effects on vegetation growth. For instance, when temperatures exceed the optimal range for vegetation growth, warming might lead to more frequent occurrences of extreme heatwaves, droughts, and wildfires in forests, negatively affecting vegetation productivity (Zhang *et al* 2022b). When elevated CO_2 leads to an increase in leaf area, it could potentially enhance transpiration leading to a faster depletion of soil moisture and consequently exacerbating the negative impacts of drought (Nowak *et al* 2004, De Kauwe *et al* 2021). Moreover, elevated atmospheric CO_2 levels can increase the sensitivity of arid vegetation to precipitation, potentially leading to decreased ecosystem stability and greater vulnerability of fragile ecosystems to the destructive effects of drought (Zhang *et al* 2022a). Other natural factors, such as precipitation and nitrogen deposition, also influence the changing GPP trends (figure 3). Wang *et al* (2018) found that an increase in precipitation can enhance the carbon sink strength. Greaver *et al* (2016) found that nitrogen cycling is becoming increasingly important in influencing ecosystems with climate change. The availability of nitrogen and soil moisture will limit the enhancement of vegetation productivity owing to increased CO_2 concentrations (Wang *et al* 2020, Hao *et al* 2022). Our findings show that from the period 2020–2060–2060–2100, under the SSP2-4.5 scenario, the regions where temperature and nitrogen deposition dominate the changes in GPP will exceed those where CO_2 and precipitation dominate (figure 3). In the SSP5-8.5 scenario, the areas dominated by CO_2 and nitrogen deposition surpass those dominated by temperature and precipitation.

Global predictions indicate that sub-Saharan Africa, Europe, and West and Northeast Asia are at risk of increased atmospheric dryness and the expansion of drylands (Huang *et al* 2016). The findings of this study have substantial implications for dryland ecosystems beyond China, especially those facing aridity-induced challenges. The identified aridity thresholds, marked by abrupt changes in productivity, soil properties, and plant diversity, present a framework applicable to other arid and semi-arid regions. The three phases observed underscored the sensitivity and vulnerability of transitional climate regions. Global studies have also shown that rising CO_2 levels are a major driver of greening (Piao *et al* 2020). The complex interplay of factors influencing vegetation growth, including global warming, aridification, and elevated CO_2 concentrations,

is a global challenge faced by drylands. This study can help understand the phenomenon of concurrent greening of atmospheric dryness in dryland ecosystems, providing scientific insights for developing targeted mitigation strategies for transitional climate regions.

While our study focused on large-scale climatic drivers and their effects on vegetation through the use of ESMs and remote sensing data, it is important to recognize that local management practices, including grazing, restoration, and deforestation, can modulate or even override the broader climatic trends we observed at the landscape or plot scale. These factors, though not explicitly modeled in our study, are critical considerations for interpreting our findings. For instance, grazing can reduce vegetation cover, alter species composition, and affect soil properties (Li *et al* 2023, Zhou *et al* 2023a), thereby influencing the vegetation's response to aridity and climate change. Vegetation restoration can mitigate the negative impacts of aridification, potentially leading to localized 'greening' trends (Zhou *et al* 2023b). We highlight the need for future research that integrates large-scale climate models with landscape or plot-scale studies that account for local management practices. This could improve the accuracy of predictions regarding vegetation dynamics and enhance the relevance of our findings for land managers and policymakers who need to consider both global climate trends and local land use practices in their decision-making processes.

5. Conclusion

This study revealed that multiple ecosystem structural and functional attributes undergo abrupt changes along aridity gradients, with critical thresholds identified at aridity levels of 0.7, 0.8, and 0.95. The anticipated expansion of certain drylands, driven by increasing aridity due to climate warming, is expected to provoke extensive modifications in ecosystem structures and functional attributes, pushing them beyond essential aridity thresholds, particularly highlighting the significance of the 0.8 aridity threshold, thus jeopardizing the sustained delivery of ecosystem services. Initially, global warming and rising CO_2 levels stimulate vegetation growth in regions that surpass aridity thresholds. However, the persistent increase in temperatures and elevated CO_2 concentrations may have detrimental effects on vegetation productivity, particularly under conditions of limited nitrogen and water availability. These transitional zones within dryland ecosystems represent ecologically vulnerable areas susceptible to aridity effects, necessitating the development of conservation strategies to mitigate aridification induced by climate change and alleviate degradation in these critical areas.

Data availability statement

The aridity index is available in the global aridity index (Global-Aridity) and global potential evapotranspiration (Global-PET) geospatial database (Trabucco and Zomer 2018). Inter-annual precipitation variability is available in the TerraClimate datasets (Abatzoglou *et al* 2018). Soil organic carbon, soil nitrogen content, and silt + clay content are available in the ISRIC-WISE Soil Property Databases (Batjes 2016). The NDVI is available for the MODIS MOD13Q1 product (Tucker and Sellers 1986). GPP is available for the MODIS MOD17A2 product (Running *et al* 2015). Vegetation cover in the MODIS MOD44B product (Justice *et al* 2002). The root-shoot ratio is available from Ma *et al* (2021). Biocrust cover is obtained from the Rodriguez-Caballero *et al* (2018). Plant species richness is obtained from Ellis *et al* (2012). The vegetation sensitivity index is obtained from Seddon *et al* (2016). The sensitivity of vegetation to precipitation is available is obtained from Li *et al* (2021). Aboveground carbon density and belowground carbon density are available in Xu *et al* (2020b). The ecosystem functions are available from Xu *et al* (2020a). The CMIP6 outputs can be downloaded from the Institute Pierre-Simon Laplace server (https://esgf-node.ipsl.upmc.fr/search/cmip6-ipsl/). FLUXCOM GPP data (Pastorello *et al* 2020) can be downloaded from http://fluxcom.org/CF-Download/. CRU/NCEP-derived climatic data can be downloaded from https://rda.ucar.edu/datasets/ds314.3/dataaccess/.

All data that support the findings of this study are included within the article (and any supplementary files).

Author contributions

Wenxin Zhou: Writing—original draft, Visualization, Formal analysis. **Changjia Li:** Writing—review & editing, Conceptualization, Funding acquisition. **Bojie Fu:** Funding acquisition. **Shuai Wang:** Conceptualization. **Zhuobing Ren:** Visualization, Formal analysis. **Lindsay C Stringer:** Writing—review & editing.

Conflict of interest

The authors declare no competing interests.

ORCID iDs

Wenxin Zhou ⦿ https://orcid.org/0000-0001-5133-7314

Changjia Li ⦿ https://orcid.org/0000-0001-7297-9658

References

Abatzoglou J T, Dobrowski S Z, Parks S A and Hegewisch K C 2018 TerraClimate, a high-resolution global dataset of monthly climate and climatic water balance from 1958–2015 *Sci. Data* **5** 1–12

Abel C, Horion S, Tagesson T, Brandt M and Fensholt R 2019 Towards improved remote sensing based monitoring of dryland ecosystem functioning using sequential linear regression slopes (SeRGS) *Remote Sens. Environ.* **224** 317–32

Batjes N H 2016 Harmonized soil property values for broad-scale modelling (WISE30sec) with estimates of global soil carbon stocks *Geoderma* **269** 61–68

Berdugo M *et al* 2020 Global ecosystem thresholds driven by aridity *Science* **367** 787–90

Berdugo M, Gaitán J J, Delgado-Baquerizo M, Crowther T W and Dakos V 2022a Prevalence and drivers of abrupt vegetation shifts in global drylands *Proc. Natl Acad. Sci.* **119** e2123393119

Berdugo M, Kéfi S, Soliveres S and Maestre F T 2017 Plant spatial patterns identify alternative ecosystem multifunctionality states in global drylands *Nat. Ecol. Evol.* **1** 0003

Berdugo M, Vidiella B, Solé R V and Maestre F T 2022b Ecological mechanisms underlying aridity thresholds in global drylands *Funct. Ecol.* **36** 4–23

Bonan G B and Doney S C 2018 Climate, ecosystems, and planetary futures: the challenge to predict life in Earth system models *Science* **359** eaam8328

Braswell B H, Schimel D S, Linder E and Moore B 1997 The response of global terrestrial ecosystems to interannual temperature variability *Science* **278** 870–3

Cavanaugh J E and Neath A A 2019 The Akaike information criterion: background, derivation, properties, application, interpretation, and refinements *WIREs Comput. Stat.* **11** e1460

D'Odorico P, Bhattachan A, Davis K F, Ravi S and Runyan C W 2013 Global desertification: drivers and feedbacks *Adv. Water Resour.* **51** 326–44

De Kauwe M G, Medlyn B E and Tissue D T 2021 To what extent can rising [CO_2] ameliorate plant drought stress? *New Phytol.* **231** 2118–24

Donohue R J, Roderick M L, McVicar T R and Farquhar G D 2013 Impact of CO_2 fertilization on maximum foliage cover across the globe's warm, arid environments *Geophys. Res. Lett.* **40** 3031–5

Ellis E C, Antill E C and Kreft H 2012 All is not loss: plant biodiversity in the Anthropocene *PLoS One* **7** e30535

Flato G M 2011 Earth system models: an overview *WIREs Clim. Change* **2** 783–800

Fu L, Zhang G, Huang J, Peng M, Ding L and Han D 2024 Prevalence of vegetation browning in China's drylands under climate change *Geogr. Sustain.* **5** 405–14

Greaver T L *et al* 2016 Key ecological responses to nitrogen are altered by climate change *Nat. Clim. Change* **6** 836–43

Hao H, Li Z, Chen Y, Xu J, Li S and Zhang S 2022 Recent variations in soil moisture use efficiency (SMUE) and its influence factors in Asian drylands *J. Clean. Prod.* **373** 133860

Higgins S I, Conradi T and Muhoko E 2023 Shifts in vegetation activity of terrestrial ecosystems attributable to climate trends *Nat. Geosci.* **16** 147–53

Hillebrand H, Donohue I, Harpole W S, Hodapp D, Kucera M, Lewandowska A M and Freund J A 2020 Thresholds for

ecological responses to global change do not emerge from empirical data *Nat. Ecol. Evol.* **4** 1–8

Hu W G *et al* 2021 Aridity-driven shift in biodiversity-soil multifunctionality relationships *Nat. Commun.* **12** 5350

Huang J *et al* 2017 Dryland climate change: recent progress and challenges *Rev. Geophys.* **55** 719–78

Huang J, Yu H, Guan X, Wang G and Guo R 2016 Accelerated dryland expansion under climate change *Nat. Clim. Change* **6** 166–71

Huang K *et al* 2018 Enhanced peak growth of global vegetation and its key mechanisms *Nat. Ecol. Evol.* **2** 1897

Jiao W, Wang L, Smith W K, Chang Q, Wang H and D'Odorico P 2021 Observed increasing water constraint on vegetation growth over the last three decades *Nat. Commun.* **12** 3777

Justice C, Townshend J, Vermote E, Masuoka E, Wolfe R, Saleous N, Morisette J and Morisette J T 2002 An overview of MODIS Land data processing and product status *Remote Sens. Environ.* **83** 3–15

Li C, Fu B, Wang S, Stringer L C, Wang Y, Li Z, Zhou W and Zhou W 2021 Drivers and impacts of changes in China's drylands *Nat. Rev. Earth Environ.* **2** 858–73

Li C, Fu B, Wang S, Stringer L C, Zhou W, Ren Z and Maestre F T 2023 Climate-driven ecological thresholds in China's drylands modulated by grazing *Nat. Sustain.* **2** 1–10

Lian X *et al* 2021 Multifaceted characteristics of dryland aridity changes in a warming world *Nat. Rev. Earth Environ.* **2** 232–50

Luo W T *et al* 2016 Thresholds in decoupled soil-plant elements under changing climatic conditions *Plant Soil* **409** 159–73

Ma H, Mo L, Crowther T W, Maynard D S, van den Hoogen J, Stocker B D, Zohner C M and Zohner C M 2021 The global distribution and environmental drivers of aboveground versus belowground plant biomass *Nat. Ecol. Evol.* **5** 1110–22

Maestre F T *et al* 2012 Plant species richness and ecosystem multifunctionality in global drylands *Science* **335** 214–8

Maestre F T *et al* 2016 Structure and functioning of dryland ecosystems in a changing world *Annu. Rev. Ecol. Evol. Syst.* **47** 215–37

Mansfield T and Freer-Smith P 1984 The role of stomata in resistance mechanisms *Gaseous Air Pollutants and Plant Metabolism* (Butterworths) pp 131–46

Manzoni S, Jackson R B, Trofymow J A and Porporato A 2008 The global stoichiometry of litter nitrogen mineralization *Science* **321** 684–6

Matson P, Kathleen A L and Hall S J 2002 The globalization of nitrogen deposition: consequences for terrestrial ecosystems *Ambio* **31** 113–9

Mirzabaev A, Wu J H, Evans J, García-Oliva F, Hussein I A G, Iqbal M H and Weltz M 2019 Desertification *Climate Change and Land: an IPCC special report on climate change, desertification, land degradation, sustainable land management, food security, and greenhouse gas fluxes in terrestrial ecosystems*

Nowak R S, Zitzer S F, Babcock D, Smith-Longozo V, Charlet T N, Coleman J S, Smith S D and Smith S D 2004 Elevated atmospheric CO_2 does not conserve soil water in the mojave desert *Ecology* **85** 93–99

O'Ishi R, Abe-Ouchi A, Prentice I C and Sitch S 2009 Vegetation dynamics and plant CO_2 responses as positive feedbacks in a greenhouse world *Geophys. Res. Lett.* **36** L11706

Pastorello G *et al* 2020 The FLUXNET2015 dataset and the ONEFlux processing pipeline for eddy covariance data *Sci Data* **7** 225

Piao S *et al* 2020 Characteristics, drivers and feedbacks of global greening *Nat. Rev. Earth Environ.* **1** 14–27

Prăvălie R, Bandoc G, Patriche C and Sternberg T 2019 Recent changes in global drylands: evidences from two major aridity databases *Catena* **178** 209–31

Reich P B, Hobbie S E and Lee T D 2014 Plant growth enhancement by elevated CO_2 eliminated by joint water and nitrogen limitation *Nat. Geosci.* **7** 920–4

Rodriguez-Caballero E, Belnap J, Büdel B, Crutzen P J, Andreae M O, Pöschl U and Weber B 2018 Dryland

photoautotrophic soil surface communities endangered by global change *Nat. Geosci.* **11** 185–9

Rohat G, Flacke J, Dao H and van Maarseveen M 2018 Co-use of existing scenario sets to extend and quantify the shared socioeconomic pathways *Clim. Change* **151** 619–36

Running S, Mu Q and Zhao M 2015 *MOD17A2H MODIS/Terra Gross Primary Productivity 8-Day L4 Global 500m SIN Grid V006* (https://doi.org/10.5067/MODIS/MOD17A2H.006)

Seddon A W, Macias-Fauria M, Long P R, Benz D and Willis K J 2016 Sensitivity of global terrestrial ecosystems to climate variability *Nature* **531** 229–32

Sellers P J *et al* 1996 Comparison of radiative and physiological effects of doubled atmospheric CO_2 on climate *Science* **271** 1402–6

Smith W K, Dannenberg M P, Yan D, Herrmann S, Barnes M L, Barron-Gafford G A and Hudson A 2019 Remote sensing of dryland ecosystem structure and function: progress, challenges, and opportunities *Remote Sens. Environ.* **233** 111401

Sugihara G, May R, Ye H, Hsieh C-H, Deyle E, Fogarty M and Munch S 2012 Detecting causality in complex ecosystems *Science* **338** 496–500

Team RDC 2008 *R: A Language and Environment for Statistical Computing*

Trabucco A and Zomer R J 2018 *Global Aridity Index and Potential Evapo-Transpiration (ET0) Climate Database v2*

Tucker C J and Sellers P 1986 Satellite remote sensing of primary production *Int. J. Remote Sens.* **7** 1395–416

van der Esch S 2017 Exploring future changes in land use and land condition and the impacts on food, water, climate change and biodiversity: scenarios for the UNCCD Global Land Outlook

Wang C, Wang X B, Liu D W, Wu H H, Lu X T, Fang Y T and Bai E 2014 Aridity threshold in controlling ecosystem nitrogen cycling in arid and semi-arid grasslands *Nat. Commun.* **5** 1–8

Wang L, Jiao W, MacBean N, Rulli M C, Manzoni S, Vico G and D'Odorico P 2022 Dryland productivity under a changing climate *Nat. Clim. Change* **12** 981–94

Wang S *et al* 2020 Recent global decline of CO_2 fertilization effects on vegetation photosynthesis *Science* **370** 1295–300

Wang X, Chen F, Hasi E and Li J 2008 Desertification in China: an assessment *Earth Sci. Rev.* **88** 188–206

Wang Y, Chen J, Zhou G, Shao C, Chen J, Wang Y and Song J 2018 Predominance of precipitation event controls ecosystem CO_2 exchange in an inner Mongolian desert grassland, China *J. Clean. Prod.* **197** 781–93

Wu B, Zeng H, Lü N, Wang Y, Fu B and Xu Z 2020 Essential dryland ecosystem variables *Curr. Opin. Environ. Sustain.* **48** 68–76

Xu J, Chen J, Liu Y and Fan F 2020a Identification of the geographical factors influencing the relationships between ecosystem services in the Belt and Road region from 2010 to 2030 *J. Clean. Prod.* **275** 124153

Xu L, He N and Yu G 2020b *Carbon density data set of Chinese terrestrial ecosystem in 2010s* (https://doi.org/10.11922/csdata.2018.0026.zh)

Yao J, Liu H, Huang J, Gao Z, Wang G, Li D, Chen X and Chen X 2020 Accelerated dryland expansion regulates future variability in dryland gross primary production *Nat. Commun.* **11** 1665

Zhang C, Yang Y, Yang D, Wang Z, Wu X, Zhang S and Zhang W 2020 Vegetation response to elevated CO_2 slows down the eastward movement of the 100th meridian *Geophys. Res. Lett.* **47** e2020GL089681

Zhang Y *et al* 2022a Increasing sensitivity of dryland vegetation greenness to precipitation due to rising atmospheric CO_2 *Nat. Commun.* **13** 4875

Zhang Y, Piao S, Sun Y, Rogers B M, Li X, Lian X, Peñuelas J, Chen A and Peñuelas J 2022b Future reversal of warming-enhanced vegetation productivity in the Northern Hemisphere *Nat. Clim. Change* **12** 581–6

Zhou W, Li C, Wang S, Ren Z and Stringer L C 2023a Effects of grazing and enclosure management on soil physical and chemical properties vary with aridity in China's drylands *Sci. Total Environ.* **877** 162946

Zhou W, Li C, Wang S, Ren Z and Stringer L C 2023b Effects of vegetation restoration on soil properties and vegetation attributes in the arid and semi-arid regions of China *J. Environ. Manage.* **343** 118186